Available online at www.sciencedirect.com
ScienceDirect
Procedia Engineering 00 (2010) 1–10
Procedia Engineering

IUTAM Symposium on Computational Aero-Acoustics
for Aircraft Noise Prediction

Flow Filtering and the Physical Sources of Aerodynamic Sound

Samuel Sinayoko, Anurag Agarwal

Highfield, Southampton SO17 1BJ, United Kingdom

Abstract

The physical sources of sound are expressed in terms of the non-radiating part of the flow. The non-radiating part of the flow can be obtained from convolution filtering, as we demonstrate numerically by using an axi-symmetric jet satisfying the Navier–Stokes equations. Based on the frequency spectrum of the source, we show that the sound sources exhibit more physical behaviour than sound sources based on acoustic analogies. To validate the sources of sound, one needs to let them radiate within the non-radiating flow field. However, our results suggest that the traditional Euler operator linearized about the time-averaged part of the flow should be sufficient to compute the sound field.

Keywords: aerodynamic sound, flow filtering, sound sources, physical sources

1. Introduction

Despite more than 50 years of research in aeroacoustics, controlling the sound radiated by turbulent jets remains difficult. One reason is that no definite answer has been found on how turbulent flows generate sound. A major obstacle is the lack of understanding of the physical sources of sound in a jet.

One way to derive the aerodynamic noise sources is to use an acoustic analogy. In an acoustic analogy, the hydrodynamic field is assumed to be independent from the acoustic field. This allows to rearrange the Navier-Stokes equations to have a linear wave-propagation operator on the left-hand side; the remaining terms are grouped as sources on the right hand side. In general, the operator is obtained by deriving the governing equations for the flow fluctuations about a steady mean-flow. Goldstein [1] provides a good generalisation of such approaches. The fluctuating variables on the left-hand-side are the dependent variables of the problem and represent both acoustic and hydrodynamic waves. This implies that the sources on the right-hand side cannot be identified as just sound sources. Furthermore, we expect the sound field to be a small by-product of the hydrodynamic field. Therefore, the sound source should be a function of the hydrodynamic field only. This property is not satisfied by traditional acoustic analogies.

An attempt to overcome these difficulties and to define the physical sources of sound is made by Goldstein [2]. He shows that if a flow field can be separated into its radiating and non-radiating components, then the resulting sound sources are mainly a function of the non-radiating components and should approach the physical sources of sound. The present paper is inspired by Goldstein's work. Our objective is to show that it is indeed possible to separate radiating acoustic components from non-radiating components in nonlinear flows.

We show that, following such a decomposition, the sound sources depend only on the non-acoustic field. The source terms do not contain the dependent acoustic variables and should therefore represent the true sources of sound. We present a simple expression for the source terms. It is similar to the one derived by Goldstein. However, we

do not use Favre averaging and our result is only approximate because we ignore entropy sources and terms which are quadratic in the acoustic variables. These choices simplify the derivation of the sources and should have little consequence for the flows we are studying here.

The paper is organised as follows. In §2, we derive the aerodynamic noise sources based on a non-radiating unsteady base flow. We restrict ourselves to isentropic flows, in which temperature effects are negligible. We show that the linear propagation operator can be approximated by the linearised Euler operator. In § 3, we decompose an axisymmetric jet into its radiating part and non-radiating part by using a convolution filter [3]. The axisymmetric jet is excited at the inflow by two frequencies and satisfies an inhomogeneous version of the Navier-Stokes equations. The non-radiating base flow is used to compute the corresponding sound sources. We use these results to validate the assumptions made in § 1.

2. Aerodynamic sound sources

2.1. Flow decomposition

We decompose the flow field into its radiating and non-radiating components. The radiating components are those which satisfy the dispersion relation $|\mathbf{k}| = |\omega|/c_\infty$ in the frequency–wavenumber domain, where $\mathbf{k}$ is the wavenumber, ω the angular frequency and c_∞ the far field speed of sound ([4, 2]). Physically, the non-radiating components are made of:

- the steady mean flow,
- the hydrodynamic fluctuations about the mean flow.

The radiating components correspond to acoustic waves. In this paper, we use the terms "acoustic field" and "radiating field" interchangeably.

For a given flow variable q, the non-radiating part $\overline{q}$ can be obtained by using a convolution filter g, i.e.

$$\overline{q}(\mathbf{x}, t) \equiv \int_{-\infty}^{+\infty} \int_{\mathcal{V}} g(\mathbf{y}, \tau) q(\mathbf{x} - \mathbf{y}, t - \tau)\ d^3\mathbf{y}\, d\tau, \tag{1}$$

where $\mathcal{V}$ denotes the entire spatial domain. To achieve this, the convolution filter must satisfy

$$G(\mathbf{k}, \omega) = \begin{cases} 0 & \text{if} \quad |\mathbf{k}| = |\omega|/c_\infty, \\ 1 & \text{if} \quad |\mathbf{k}| \neq |\omega|/c_\infty, \end{cases} \tag{2}$$

where G is the four-dimensional Fourier transform of g, defined as

$$G(\mathbf{k}, \omega) \equiv \int_{-\infty}^{+\infty} \int_{\mathcal{V}} g(\mathbf{x}, t) e^{i(\omega t - \mathbf{k}\cdot\mathbf{x})}\, d^3\mathbf{x}\, dt. \tag{3}$$

The flow variable q can then be written as

$$q = \overline{q} + q', \tag{4}$$

where q' represents the radiating components of the flow.

2.2. Source definition

The flow variables satisfy the Navier–Stokes equations:

$$\frac{\partial \rho}{\partial t} + \frac{\partial \rho v_j}{\partial x_j} = 0, \tag{5}$$

$$\frac{\partial \rho v_i}{\partial t} + \frac{\partial \rho v_i v_j}{\partial x_j} + \frac{\partial p}{\partial x_i} = \frac{\partial \sigma_{ij}}{\partial x_j}, \tag{6}$$

where ρ, p and $\mathbf{v} = (v_i)$ denote the density, pressure and flow velocity, and σ_{ij} the viscous stress tensor. If we assume that the flow is isentropic and is a perfect gas, then (from Goldstein [5])

$$\frac{\partial p}{\partial t} + u_j \frac{\partial p}{\partial x_j} + \gamma p \frac{\partial u_j}{\partial x_j} = 0. \tag{7}$$

Introducing the variable $\pi = (p/p_\infty)^{1/\gamma}$, in which p_∞ is the pressure in the ambient medium, allows us to rewrite (6) and (7) in conservative form (Lilley[6]):

$$\frac{\partial \rho v_i}{\partial t} + \frac{\partial \rho v_i v_j}{\partial x_j} + p_\infty \frac{\partial \pi^\gamma}{\partial x_i} = 0 \tag{8}$$

$$\frac{\partial \pi}{\partial t} + \gamma \frac{\partial \pi u_j}{\partial x_j} = 0. \tag{9}$$

Let $\mathcal{L}$ denote the linear operator associated with the convolution filter of (1). For each term in the above equations, the radiating part can be obtained by applying the linear filter $\mathcal{L}' \equiv \mathcal{I} - \mathcal{L}$, where $\mathcal{I}$ denotes the identity operator. Applying $\mathcal{L}'$ to (5), (8) and (9) gives the governing equations for the radiating components:

$$\frac{\partial \rho'}{\partial t} + \frac{\partial (\rho v_j)'}{\partial x_j} = 0, \tag{10}$$

$$\frac{\partial (\rho v_i)'}{\partial t} + \frac{\partial (\rho v_i v_j)'}{\partial x_j} + p_\infty \frac{\partial (\pi^\gamma)'}{\partial x_i} = \frac{\partial \sigma'_{ij}}{\partial x_j}, \tag{11}$$

$$\frac{\partial \pi'}{\partial t} + \gamma \frac{\partial (\pi u_j)'}{\partial x_j} = 0. \tag{12}$$

The viscous term in (11) does not play a significant role in sound generation for the type of flows we are interested in. It provides a very small amount of dissipation that can be neglected.

We rewrite each of the above equations to obtain: (a) an operator that is linear in the radiating variables (ρ', v_i' and π') on the left hand side, (b) a source term on the right hand side. For example, in (11), the term $\rho v_i v_j$ can be expanded as

$$\rho v_i v_j = \overline{\rho}\,\overline{v_i}\,\overline{v_j} + \overline{v_i}\,\overline{v_j}\rho' + \overline{\rho}\,\overline{v_j}\,v_i' + \overline{\rho}\,\overline{v_i}\,v_j' + O(\rho'^2), \tag{13}$$

where $O(\rho'^2)$ represents terms that are quadratic in acoustic quantities. Because the radiating part of the flow is normally several orders of magnitude smaller than the non-radiating part, these quadratic components are expected to be small. Applying $\mathcal{L}'$ to (13) gives

$$(\rho v_i v_j)' = \underbrace{(\overline{\rho}\,\overline{v_i}\,\overline{v_j})'}_{\text{(a)}} + \underbrace{(\overline{v_i}\,\overline{v_j}\rho' + \overline{\rho}\,\overline{v_j}\,v_i' + \overline{\rho}\,\overline{v_i}\,v_j')'}_{\text{(b)}} + O(\rho'^2)'. \tag{14}$$

We assume a one-way coupling between hydrodynamics and acoustics: the hydrodynamic field is responsible for the production of sound but the sound field does not affect the hydrodynamic field. The source of sound must therefore be independent of the fluctuating components. The only terms satisfying this requirement are those in group (a), which are non-linear in hydrodynamic quantities. The terms in group (b) involve an acoustic component interacting with the non-radiating base flow. These terms represent propagation effects such as refraction and should be excluded from the source. Similarly, the other non-linear terms in equations (10–12) are decomposed as follows:

$$(\rho v_i)' \approx (\overline{\rho}\,\overline{v_i})' + (\overline{v_i}\rho' + \overline{\rho}\,v_i')', \tag{15}$$

$$(\pi v_j)' \approx (\overline{\pi}\,\overline{v_j})' + (\overline{v_j}\pi' + \overline{\pi}\,v_j')', \tag{16}$$

$$(\pi^\gamma)' \approx (\overline{\pi^\gamma})' + \gamma(\overline{\pi^{\gamma-1}}\pi')' = \gamma(\overline{\pi^{\gamma-1}}\pi')'. \tag{17}$$

In each of the above equations, the first term on the right hand side is the source of sound. The higher order terms have been neglected. We can now rewrite equations (10–12) by pushing the sound sources to the right hand side:

$$\frac{\partial \rho'}{\partial t} + \frac{\partial}{\partial x_j}(\overline{v_j}\rho' + \overline{\rho}\, v_j')' = m, \tag{18}$$

$$\frac{\partial}{\partial t}(\overline{v_i}\rho' + \overline{\rho}\, v_i')' + \frac{\partial}{\partial x_j}(\overline{v_i}\,\overline{v_j}\rho' + \overline{\rho}\,\overline{v_j}\, v_i' + \overline{\rho}\,\overline{v_i}\, v_j')' + \gamma p_\infty \frac{\partial}{\partial x_i}(\overline{\pi^{\gamma-1}}\pi') = f_i, \tag{19}$$

$$\frac{\partial \pi'}{\partial t} + \gamma \frac{\partial}{\partial x_j}(\overline{\pi}\, v_j' + \pi'\,\overline{v_j})' = e, \tag{20}$$

where the continuity equation source term l, the momentum equation source term f_i and the energy equation source term e are defined as

$$m \equiv -\frac{\partial}{\partial x_j}(\overline{\rho}\,\overline{v_j})', \tag{21}$$

$$f_i \equiv -\frac{\partial}{\partial t}(\overline{\rho}\,\overline{v_i})' - \frac{\partial}{\partial x_j}(\overline{\rho}\,\overline{v_i}\,\overline{v_j})', \tag{22}$$

$$e \equiv -\gamma \frac{\partial}{\partial x_j}(\overline{\pi}\,\overline{v_j})'. \tag{23}$$

These equations show that the sound sources m, f_i and e are all radiating quantities; this is what we expect because the operator on the left hand side of (18–20) is a linear function of the radiating variables. It means that these sources produce only acoustic waves. Also, as we expect from the sound sources, they are expressed as (nonlinear) functions of only the non-radiating components: they are free of the dependant (acoustic) variables. Therefore, these sources should represent the true sources of aerodynamically generated sound. These key features distinguish the present source from past representations based on acoustic analogies.

2.3. Physical interpretation for the propagation operator

The the left hand side of equations (10–12) contain terms of the form $(f(\rho', v_i', \pi'))'$, where the f is a linear function of the radiating variables. These terms depend of the filter that is used which prevents us to provide a general physical interpretation for the left hand side of equations (10–12).

However, each non radiating term $\overline{q}$, (e.g $\overline{\pi}$), can be decomposed into a steady mean part q_0 and an unsteady part $\tilde{q}$, i.e.

$$\overline{q} = q_0 + \tilde{q}. \tag{24}$$

The unsteady part $\tilde{q}$ represents hydrodynamic components. If we assume that

$$q' \ll \tilde{q} \ll q_0, \tag{25}$$

then we can derive the dominant terms on the left hand side of equations (10–12). For example, the term $(\overline{v}_i\rho')'$ can be decomposed as

$$(\overline{v}_i\rho')' = (v_{i0}\rho')' + (\tilde{v}_i\rho')' = v_{i0}\rho' + (\tilde{v}_i\rho')'. \tag{26}$$

The second equality is true because the $v_{i0}\rho'$ is a purely radiating term. Furthermore, the radiating term "$(\tilde{v}_i\rho')'$" can be neglected because, from (25),

$$(\tilde{v}_i\rho')' \ll \tilde{v}_i\rho' \ll v_{i0}\rho'. \tag{27}$$

Therefore

$$(\overline{v}_i\rho')' \approx v_{i0}\rho'. \tag{28}$$

This example shows that the interaction terms between radiating and non-radiating components reduce to interactions between the radiating components and the steady mean flow. Using this reasoning, equations (10–12) can be

approximated by

$$\frac{\partial \rho'}{\partial t} + \frac{\partial}{\partial x_j}(v_{j0}\rho' + \rho_0 v_j')' = m, \tag{29}$$

$$\frac{\partial}{\partial t}(v_{i0}\rho' + \rho_0 v_i')' + \frac{\partial}{\partial x_j}(v_{i0} v_{j0}\rho' + \rho_0 v_{j0} v_i' + \rho_0 v_{i0} v_j')' + \gamma p_\infty \frac{\partial}{\partial x_i}(\overline{\pi^{\gamma-1}}\pi') = f_i, \tag{30}$$

$$\frac{\partial \pi'}{\partial t} + \gamma \frac{\partial}{\partial x_j}(\pi_0 v_j' + \pi' v_{j0})' = e, \tag{31}$$

which are inhomogeneous Euler equations linearised about a steady base flow. The source terms remain unchanged and are those defined in (21–23). This result suggests that, once the sources of sound have been derived, the sound can be propagated by using an inhomogeneous version of the linearised Euler equations.

2.4. Wave equation

The sound source we have obtained takes the form of a vector whose components are m, f_i and e. It is also possible to write the source in the form of a scalar expression. We can obtain an inhomogeneous wave equation by computing $\partial\mathcal{L}'(18)/\partial x_i - \partial\mathcal{L}'(19)/\partial t$, which gives

$$\gamma p_\infty \frac{\partial^2(\overline{\pi^{\gamma-1}}\pi')}{\partial x_i \partial x_i} - \frac{\partial^2 \rho'}{\partial t^2} + \frac{\partial^2}{\partial x_i \partial x_j}(\overline{v_i}\,\overline{v_j}\rho' + \overline{\rho}\,\overline{v_j} v_i' + \overline{\rho}\,\overline{v_i} v_j')' = \frac{\partial^2}{\partial x_i \partial x_j} s_{ij} \tag{32}$$

where s_{ij} is defined as

$$s_{ij} \equiv -(\overline{\rho}\,\overline{v_i}\,\overline{v_j})' = -\left(\overline{\rho}\,\overline{v_i}\,\overline{v_j} - \overline{\overline{\rho}\,\overline{v_i}\,\overline{v_j}}\right). \tag{33}$$

As we expect from the physical source of sound, s_{ij} is a function of the non-radiating variables only and is itself purely radiating. Secondly we note that equation (A.2) reduces to the homogeneous second order wave equation in the ambient medium.

The terms of the form $(\overline{\rho} v_i)'$, which are present in both m and f_i, cancel out in s_{ij}.

3. Sources of sound in an axi-symmetric jet flow

3.1. Problem description

We now consider a nonlinear problem in which an axi-symmetric jet is excited by two discrete-frequency axi-symmetric disturbances at the jet exit. The frequencies are chosen to trigger some instability waves in the flow. These instability waves grow downstream and interact non-linearly, generating acoustic waves. The Mach number of the jet is 0.9 and the Reynolds number is 3600. The base mean flow is chosen to match the experimental data of Stromberg *et al.* [7].

Suponitsky and Sandham [8] performed direct numerical simulations of the compressible Navier–Stokes equations for this problem. In their simulations the mean flow was prescribed by imposing time-independent forcing terms. They ran simulations with different combinations of excitation frequencies and amplitudes. The data used here corresponds to the combination with the largest acoustic radiation. The two excitation frequencies are $\omega_1 = 2.4$ and $\omega_2 = 3.4$. The results presented in this section have been normalised by using the jet diameter D, jet exit speed U_j and the ambient density as the length, velocity and density scales, respectively.

3.2. Flow decomposition

In order to apply the convolution filtering technique for flow decomposition, we first need to obtain the Fourier transform (FT) of the flow field. In general this involves transforming in four (time and 3 space) dimensions. However, given the axi-symmetric nature of the present problem, we are able to do the spatial transforms in two dimensions: by applying a Hankel transform (HT) in the radial direction and a Fourier transform in the axial direction. The Hankel transform is carried out numerically by using the quasi-discrete Hankel transform described by Guizar-Sicairos and Guitiérrez-Vega [9].

For a given flow variable q, the algorithm for obtaining the non-radiating variable $\overline{q}$ is as follows:

- interpolate and zero pad the data (to avoid aliasing) in the physical space,
- compute and remove the time-averaged variable q_0
- compute the FT in the axial direction and the HT in the radial direction,
- multiply by the filter window G,
- compute the inverse Hankel transform and the inverse Fourier transform,
- unpad the data and add back q_0.

Mathematically, the filtering procedure can be written as

$$\overline{q} = q_0 \quad + \quad \mathrm{HT}^{-1} \circ \mathrm{FT}^{-1}\Big(\mathrm{HT} \circ \mathrm{FT}(q - q_0) \times G\Big) \tag{34}$$

The window G should satisfy equation (2). For a given frequency ω, we want G to have a value of 0 in a narrow band around $|\mathbf{k}| = |\omega|/c_\infty = k_{co}$ and of 1 everywhere else. We use a narrow Butterworth band-reject filter to achieve this:

$$G(\mathbf{k}) = \left(1 + \frac{|\mathbf{k}|\sigma}{|\mathbf{k}|^2 - k_{co}^2}\right)^{-4}, \tag{35}$$

where σ controls the width of the stop-band and k_{co} is the cut-off frequency. In the present problem, the noise radiates mainly at the difference frequency, $\Delta w = \omega_2 - \omega_1$. For this frequency, $k_{co} = 1.2$. We choose a value of 0.25 for σ.

Results and discussion

The success of the filtering operation is verified by examining the fluctuating part of the pressure field ($p' = p - \bar{p}$), which should contain no hydrodynamic components. Figures 1(a) and 1(b) respectively show total pressure p (excluding low frequency components p_0), and fluctuating pressure p'. They demonstrate that a clear identification of the radiating components has been achieved since p' contains no hydrodynamic component. This shows that using this filtering procedure we are able to obtain the filtered field to a very high order of accuracy because we are subtracting two large quantities (p and $\overline{p}$) to obtain a much smaller quantity (p'). More precisely, we find that p' is three orders of magnitude smaller than $\overline{p}$ along the jet centerline, and $\tilde{p} = \overline{p} - p_0$ is two orders of magnitude smaller than p_0. Similar results have been obtained using the same filter for the other flow variables. This validates the hypotheses that acoustics are much smaller than hydrodynamics, and hydrodynamics are much smaller than time-averaged components. These hypotheses are commonly used in the aeroacoustics community and are used in the derivation of (28).

The above filtering procedure is equivalent to convolving the flow with a mask. In the vicinity of the boundary, a part of the mask will lie outside the computational domain where the flow is set to zero due to zero-padding. This leads to inaccuracies near boundaries. To restrict this effect to small regions, the filter must be narrow in the space–time domain. Unfortunately, optimal non-radiating filters must also be narrow in the wavenumber–frequency domain, which is impossible. A trade-off must be made between these two requirements. As can be seen in figure 1, p' is over-estimated in the first 4 jet diameters. One possible solution would be to extend the computational domain upstream in the simulations.

3.3. Sound sources

The source $s_1 \equiv \partial^2 S_{ij}/\partial x_i \partial x_j$ associated with the non-radiating filter defined in the previous section is computed using the double divergence of (33). Figure 2(a) shows the source for $0 \le r \le 2.0$ and $0 \le z \le 18$. For comparison, the source s_2 associated with a classic decomposition using a time-averaged base flow is given in figure 2(b). As shown in appendix A,

$$s_2 \equiv -\frac{\partial^2}{\partial x_i \partial x_j}(\rho_0 v_i'' v_j'' + v_{i0}\rho'' v_i'' + v_{j0}\rho'' v_i'')'' \tag{36}$$

where the double primes denote fluctuations about the mean.

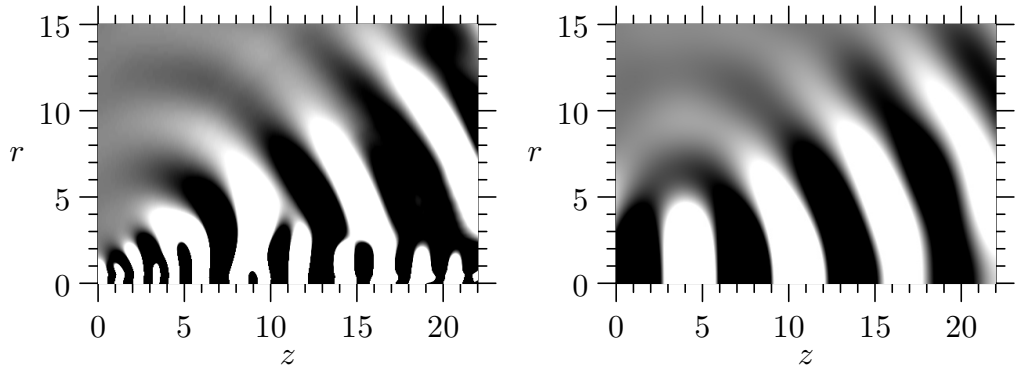

(a) Total pressure p

(b) Fluctuating pressure $p' = p - \overline{p}$

Figure 1: Pressure fields for a single time frame. In (a), low frequency components p_0 have been removed for plotting. The linear contour scale ranges from $-5 \cdot 10^{-6}$ (black) to $5 \cdot 10^{-6}$ (white).

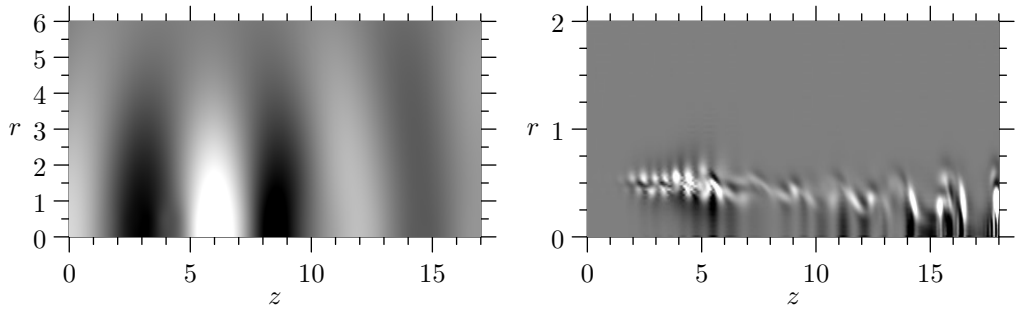

(a) Sound source s_1 associated with a non-radiating base flow.

(b) Sound source s_2 associated with a time-averaged base flow.

Figure 2: Sound sources for a single time frame. The contour scale ranges from $-2 \cdot 10^{-5}$ (black) to $2 \cdot 10^{-5}$ (white) in (a) and $-5 \cdot 10^{-2}$ (black) to $5 \cdot 10^{-2}$ (white) in (b).

The source distribution is different in the two cases. With the non-radiating base flow, the source s_1 is spread over the first 4 jet diameters in the radial direction, and peaks around $z = 6$ in the axial direction, which corresponds to the end of the potential core. The source decays for $z >= 10$. With the time averaged base flow, the source (s_2) is spread along the shear layer ($r = 0.5$). In terms of amplitude, the peak value of s_2 is three orders of magnitude greater than that of s_1. This can be explained as follows: since s_1 is purely radiating (from (33)), it does not contain any hydrodynamic component, which is not the case for s_2. These hydrodynamic components are also three orders of magnitude greater than the acoustic components, as explained in § 3.2. The source s_2 drives both hydrodynamics and acoustics, whereas s_1 only generates acoustics.

Further physical insight can be obtained by looking at the power spectral density (PSD) of those sources. Figure 3(a) shows the PSD of source s_1 for $r = 0$, where s_1 is maximum as can be seen in figure 2(a). Figure 3(b) shows the PSD of s_2 for $r = 0.5$, where s_2 is dominant. These figures indicate that s_1 is dominated by the frequency $\Delta\omega = 1.2$, whereas s_2 contains several other frequencies, e.g. $\omega_1 = 2.2$, $\omega_2 = 3.4$, $2\omega_1 = 4.4$ and $\omega_1 + \omega_2 = 5.6$. We expect the true source of sound to have the frequency of acoustic waves, i.e. $\Delta\omega$. In that respect, the source s_1 based on a non-radiating base flow is more physical than s_2 which is based on a time-averaged base flow. Only a small portion of s_2 generates acoustic waves.

3.4. Validation

Equations (29–31) was assumed to be a good approximation for equations (18–20). This is tested by comparing the divergence terms on the left hand side of these equations. We use the L_∞–norm, $|q|_\infty = \max |q(\mathbf{x})|$, where $q(\mathbf{x})$ is

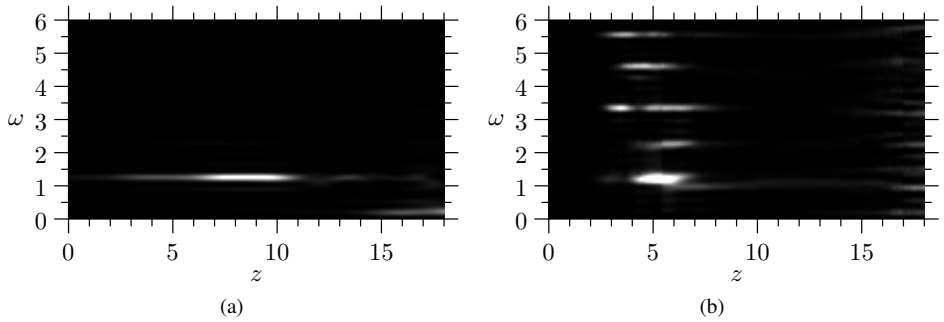

Figure 3: Power spectral density for: (a) Source s_1 (non-radiating base flow) along $r = 0$, (b) Source s_2 (time-averaged base flow) along $r = 0.5$. The contour scale ranges from 0 (black) to 2×10^{-5} (white) in (a) and 0 (black) to 5×10^{-3} (white) in (b).

evaluated over the entire grid, and we compute the relative error $\mathcal{E}$ as

$$\mathcal{E}(q_{exact}, q_{approx}) = \frac{\left|q_{exact} - q_{approx}\right|_\infty}{|q_{exact}|_\infty} \tag{37}$$

Continuity equation

Table 1 shows the relative error $\mathcal{E}$ for the continuity equation, for the terms involving velocity v_1 (left) and v_2 (right). It shows that the error is less than 0.3% for all the terms which do not involve $\overline{v_2}$. This means that (25) does not hold for $q = v_2$. This is because the jet mean flow in the radial direction, v_{20}, is very small. However, in terms of amplitude, $\overline{v_2}\rho'$ is negligible compared to $\overline{\rho}v_2'$ so that the $\rho_0 v_2' + v_{20}\rho'$ is a good approximation for $\overline{\rho}v_2' + \overline{v_2}\rho'$.

The error introduced by approximating (18) by (29) is small:

$$\mathcal{E}\left(\frac{\partial}{\partial x_j}(\overline{v_j}\rho' + \overline{\rho}\, v_j')', \frac{\partial}{\partial x_j}(v_{j0}\rho' + \rho_0 v_j')\right) = 2.7 \times 10^{-3}. \tag{38}$$

Exact	Approximation	Error
$\overline{v_1}\rho'$	$v_{10}\rho'$	1.8×10^{-3}
$\overline{\rho}v_1'$	$\rho_0 v_1'$	2.1×10^{-3}
$\overline{v_1}\rho' + \overline{\rho}v_1'$	$v_{10}\rho' + \rho_0 v_1'$	2.0×10^{-3}

Exact	Approximation	Error
$\overline{v_2}\rho'$	$v_{20}\rho'$	1.0
$\overline{\rho}v_2'$	$\rho_0 v_2'$	2.7×10^{-3}
$\overline{v_2}\rho' + \overline{\rho}v_2'$	$v_{20}\rho' + \rho_0 v_2'$	2.7×10^{-3}

Table 1: Linearised Euler approximation: divergence terms in the continuity equation

Axial momentum equation

For the axial momentum equation ($i = 1$ in (19)), the error is shown in table 2 for the terms involving the velocity and density fields. The top table shows the terms that have to be differentiated in the axial direction and the bottom one the terms that have to be differentiated in the radial direction. We observe similar results as for the continuity equation: the approximation is accurate except for the two terms involving $\overline{v_2}$. However these terms are small compared to other terms.

The error introduced by approximating (19) by (30), for $i = 1$, is given by

$$\mathcal{E}\left(\frac{\partial}{\partial x_j}(\overline{v_1}\,\overline{v_j}\rho' + \overline{\rho}\,\overline{v_j}\,v_1' + \overline{\rho}\,\overline{v_1}\,v_j')', \frac{\partial}{\partial x_j}(v_{10}\,v_{j0}\rho' + \rho_0\,v_{j0}\,v_1' + \rho_0\,v_{10}\,v_j')' + \right) = 3.3 \times 10^{-3} \tag{39}$$

Exact	Approximation	Error
$\overline{\rho}\,\overline{v_1}v_1'$	$\rho_0 v_{10} v_1'$	2.8×10^{-3}
$\overline{v_1}^2\rho'$	$v_{10}^2\rho'$	8.7×10^{-3}
$2\overline{\rho}\,\overline{v_1}v_1' + \overline{v_1}^2\rho'$	$2\rho_0 v_{10} v_1' + v_{10}^2\rho'$	2.7×10^{-3}

Exact	Approximation	Error
$\overline{\rho}\,\overline{v_1}v_2'$	$\rho_0 v_{10} v_2'$	2.8×10^{-3}
$\overline{\rho}\,\overline{v_2}v_1'$	$\rho_0 v_{20} v_1'$	1.02
$\overline{v_1}\,\overline{v_2}\rho'$	$v_{10} v_{20}\rho'$	1.02
$\overline{\rho}\,\overline{v_1}v_2' + \overline{\rho}\,\overline{v_2}v_1' + \overline{v_1}\,\overline{v_2}\rho'$	$\rho_0 v_{10} v_2' + \rho_0 v_{20} v_1' + v_{10} v_{20}\rho'$	3.3×10^{-3}

Table 2: Linearised Euler approximation: divergence terms in the axial momentum equation

Radial momentum equation

For the radial momentum equation ($i = 2$ in (19)), the error is shown in table 3 for the terms involving the velocity and density fields. The top table shows the terms that have to be differentiated in the axial direction and the bottom one the terms that have to be differentiated in the radial direction. In the bottom table, all terms involve $\overline{v_2}$ which cannot be approximated properly by v_{20}: in this case, the approximation does not give a satisfactory result.

Indeed, the error introduced by approximating (19) by (30) for $i = 2$ is given by

$$\mathcal{E}\left(\frac{\partial}{\partial x_j}(\overline{v_2}\,\overline{v_j}\rho' + \overline{\rho}\,\overline{v_j}\,v_2' + \overline{\rho}\,\overline{v_2}\,v_j')', \frac{\partial}{\partial x_j}(v_{20}\,v_{j0}\rho' + \rho_0\,v_{j0}\,v_2' + \rho_0\,v_{20}\,v_j')'\right) = 0.57 \tag{40}$$

The above error is large. However, the divergence term in the axial momentum equation is much larger than the divergence term in the radial direction:

$$\left|\frac{\partial}{\partial x_j}(\overline{v_1}\,\overline{v_j}\rho' + \overline{\rho}\,\overline{v_j}\,v_1' + \overline{\rho}\,\overline{v_1}\,v_j')'\right|_\infty = 1.4 \times 10^{-4} \tag{41}$$

$$\left|\frac{\partial}{\partial x_j}(\overline{v_2}\,\overline{v_j}\rho' + \overline{\rho}\,\overline{v_j}\,v_2' + \overline{\rho}\,\overline{v_2}\,v_j')'\right|_\infty = 2.1 \times 10^{-6} \tag{42}$$

This means that, although our approximation is inaccurate for the radial momentum equation, the propagation effects are strongest in the axial direction where our approximation is very good. Therefore, we expect the sound field obtained by using the approximate equations (29–31) to be close to the original sound field.

Exact	Approximation	Error
$\overline{\rho}\,\overline{v_2}v_1'$	$\rho_0 v_{20} v_1'$	1.02
$\overline{\rho}\,\overline{v_1}v_2'$	$\rho_0 v_{10} v_2'$	2.8×10^{-3}
$\overline{v_1}\,\overline{v_2}\rho'$	$v_{10} v_{20}\rho'$	1.02
$\overline{\rho}\,\overline{v_2}v_1' + \overline{\rho}\,\overline{v_1}v_2' + \overline{v_1}\,\overline{v_2}\rho'$	$\rho_0 v_{20} v_1' + \rho_0 v_{10} v_2' + v_{10} v_{20}\rho'$	3.3×10^{-3}

Exact	Approximation	Error
$\overline{\rho}\,\overline{v_2}v_2'$	$\rho_0 v_{20} v_2'$	1.01
$\overline{v_2}^2\rho'$	$v_{20}^2\rho'$	1.00
$2\overline{\rho}\,\overline{v_2}v_2' + \overline{v_2}^2\rho'$	$2\rho_0 v_{20} v_2' + v_{20}^2\rho'$	1.01

Table 3: Linearised Euler approximation: divergence terms in the radial momentum equation

4. Conclusion

We find that it is possible to decompose the flow field of a jet into its radiating and non-radiating parts. This can be done by using convolution filters implemented in the Fourier domain. We can thereafter obtain the physical sources of sound, which depend only on the non-radiating part of the flow. We find these sources of sound to be very different from the sources based on acoustic analogies. In particular, their amplitude is much smaller and is close to the amplitude of the sound waves in the near-field. In addition, the frequency content of the physical sources reflects that of the sound field. We find that the Euler operator linearized about the steady part of the flow can be used to propagate the physical sound sources with reasonable accuracy. This will avoid the need to solve the exact propagation equations to validate the physical sources of sound.

Acknowledgements

We are indebted to Dr. Victoria Suponitsky and Professor Neil Sandham, who carried out the DNS simulation used in this paper. We would like to thank Professor Paul White and Drs. Gwénaël Gabard and Peter Jordan for many useful discussions. This project is funded by the Engineering and Physical Sciences Research Council under grant EP/F003226/1. The authors also gratefully acknowledge Rolls-Royce plc for their financial support.

References

[1] M. Goldstein, A generalized acoustic analogy, Journal of Fluid Mechanics 488 (2003) 315 – 33.
[2] M. E. Goldstein, On identifying the true sources of aerodynamic sound, Journal of Fluid Mechanics 526 (2005) 337 – 347.
[3] S. Sinayoko, A. Agarwal, Z. Hu, On separating propagating and non-propagating dynamics in fluid-flow equations, AIAA paper 2009-3381.
[4] D. G. Crighton, Basic principles of aerodynamic noise generation, Progress in Aerospace Sciences 16 (1975) 31–96.
[5] M. Goldstein, Aeroacoustics, McGraw-Hill International Book Co., 1976.
[6] G. Lilley, The Generation and Radiation of Supersonic Jet Noise. Vol. IV - Theory of Turbulence Generated Jet Noise, Noise Radiation from Upstream Sources, and Combustion Noise. Part II: Generation of Sound in a Mixing Region, US Air Force Aero Propulsion Lab., AFAPL-TR-72-53, July.
[7] J. Stromberg, D. McLaughlin, T. Troutt, Flow field and acoustic properties of a Mach number 0.9 jet at a low Reynolds number, Journal of Sound and Vibration 72 (2) (1980) 159–176.
[8] V. Suponitsky, N. D. Sandham, Nonlinear mechanisms of sound radiation in a subsonic flow, AIAA paper 2009-3317.
[9] M. Guizar-Sicairos, J. Gutiérrez-Vega, Computation of quasi-discrete Hankel transforms of integer order for propagating optical wave fields, Journal of the Optical Society of America A 21 (1) (2004) 53–58.

Appendix A. Sources of sound for a time-averaged base flow

A classic flow decomposition method is to use a time averaged base flow. Sources based on a time-averaged base flow can be derived as follows. The flow variable q is decomposed as

$$q = q_0 + q'' \tag{A.1}$$

where q_0 and q'' denote respectively the steady and unsteady part of q.

Since taking the time average is a linear operation, following the procedure of section 2.2 leads to

$$\frac{\partial^2 p''}{\partial x_i \partial x_i} - \frac{\partial^2 \rho''}{\partial t^2} + \frac{\partial^2 (\rho v_i v_j)''}{\partial x_i \partial x_j} = 0, \tag{A.2}$$

where we have neglected the viscous term. The term $(\rho v_i v_j)''$ can be decomposed as

$$(\rho v_i v_j)'' = \underbrace{(\rho_0 \, v_{i0} \, v_{j0})''}_{(a)} + \underbrace{(v_{i0} \, v_{j0} \, \rho'' + \rho_0 \, v_{j0} \, v_i'' + \rho_0 \, v_{i0} \, v_j'')''}_{(b)} + \underbrace{(v_{i0} v_j'' \rho'' + v_{j0} v_i'' \rho'' + \overline{\rho} v_i'' v_j'')''}_{(c)} + O(\rho''^3) \tag{A.3}$$

Term (a) vanishes whereas term (b) describes interactions between the mean flow and the unsteady components, i.e. propagation effects. The sources must lie within the quadratic terms in (c). The terms in (c) are therefore considered to be the sound sources and are pushed to the right hand side of the wave equation:

$$\frac{\partial^2 p''}{\partial x_i \partial x_i} - \frac{\partial^2 \rho''}{\partial t^2} + \frac{\partial^2}{\partial x_i \partial x_j}(\, v_{i0} \, v_{j0} \, \rho'' + \, \rho_0 \, v_{j0} \, v_i'' + \, \rho_0 \, v_{i0} \, v_j'' \,) = \frac{\partial^2 T_{ij}}{\partial x_i \partial x_j}, \tag{A.4}$$

where

$$T_{ij} \equiv -(\rho_0 v_i'' v_j'' + v_{i0} \rho'' v_j'' + v_{j0} \rho'' v_i'')'' \tag{A.5}$$